J. Earth Syst. Sci. (2022)131 162
https://doi.org/10.1007/s12040-022-01903-3

Neoarchean crust–mantle interactions from the Eastern Dharwar Craton: Insights from mineral chemistry of the Nizamabad granites, southern India

Balaboina Vikram Raju[1,2], Ajay Dev Asokan[1], Rohit Pandey[3], Arathi G Panicker[1,2] and M Ram Mohan[1,2,*]

[1] *CSIR-National Geophysical Research Institute, Hyderabad 500 007, India.*
[2] *Academy of Scientific and Innovative Research, Ghaziabad 201 002, India.*
[3] *Department of Geology, Centre for Advanced Study, Institute of Science, Banaras Hindu University, Varanasi, India.*
**Corresponding author. e-mail: rammohan@ngri.res.in*

MS received 15 June 2021; revised 7 February 2022; accepted 21 February 2022

We present field, petrographic and mineral compositions of biotite, amphibole, and feldspars from Neoarchean Nizamabad granites from the northeastern part of the Eastern Dharwar Craton, southern India. These granites are classified as hornblende biotite granite (HBG), biotite granite (BTG), monzogranite (MG), and microgranular enclaves (ME) hosted in HBG and BTG. The temperature estimates using amphibole and biotite thermometry exhibit similar results, with higher temperatures for HBG (818 to 859 ±22°C) and ME (800 to 855 ±22°C), and slightly lower temperatures for BTG and MG (829 to 830 ±12°C and 820 to 829 ±12°C). Based on barometry, HBG amphiboles crystallized at pressures between 363 and 448 ±60 MPa (avg. $P_{HBG} = 398$ MPa), whereas the MEs crystallized at pressures between 313 and 438 ±60 MPa (avg. $P_{ME} = 386$ MPa). The estimated pressures suggest that these granites crystallized at depths of 14–15 km, corresponding to the upper to mid-continental crust. The amphibole compositions reveal that these granites crystallized from a water-rich magma, with >5 wt.% H_2O and evolved under high oxidizing conditions NNO + 2 (Nickel–Nickel–Oxide), corresponding to magnetite (oxidized) series granites. The amphibole and biotite compositions suggest a crust-mantle mixed source for HBG, ME, and BTG, while the MG is purely crustal derived. The water-rich and highly oxidizing conditions of the parental magmas rule out a lower crustal granulitic source for the Nizamabad granites. The amphibole and biotite compositions suggest their crystallization from calc-alkaline parental magma in a subduction setting at high oxygen fugacity (fO_2) conditions. This study infers the role of convergent margin tectonics in the emplacement of these granites, and their compositional variability is attributed to crust–mantle interactions in this domain of the Eastern Dharwar Craton.

Keywords. Granites; crystallization; Eastern Dharwar Craton; mineral chemistry; oxygen fugacity; thermobarometry.

Supplementary material pertaining to this article is available on the *Journal of Earth System Science* website (http://www.ias.ac.in/Journals/Journal_of_Earth_System_Science).

Published online: 20 July 2022

1. Introduction

The temporal changes in the mechanism(s) of continental crust extraction from the mantle are a consequence of Earth's cooling and differentiation (Laurent *et al.* 2014). The genesis of continental material started very early in the Earth's history, as demonstrated by the Hadean ages (4.0–4.4 Ga) of the Acasta gneisses, Canada (Bowring and Williams 1999) and the Jack Hills, Australia (Wilde *et al.* 2001). Continental crust has been formed continuously since then, but the growth rates and mechanisms have changed over time (Armstrong 1981; Belousova *et al.* 2010). The most important changes occurred between 3.0 and 2.5 Ga, at the Archaean–Proterozoic transition (Dhuime *et al.* 2012). Available detrital zircon age data suggest that at least ∼60–70% of the present volume of the continental crust had been generated by 3.0 Ga (Belousova *et al.* 2010; Dhuime *et al.* 2012). The widespread occurrence of granitoids in continental setting and their origin is important to understand the crustal evolution and geodynamic processes operated during the Earth's history. The generation of the huge volume of granitoids on the continental crust is due to orogenic processes either by subduction or collision (Laurent *et al.* 2014). The genetic classification of granitoids is mainly based on the amount of crust or mantle components or crust–mantle interactions involved in their genesis (Barbarin and Didier 1992; Chappell and White 1992; Chappell 1999; Altherr *et al.* 2000; Chen *et al.* 2002). The temporal and secular geochemical variations of granitoids provide a strong basis for understanding the nature, source, and physico-chemical conditions of felsic magmatism and the tectonic environment in which they were formed.

Amphibole and biotite are the commonly used ferromagnesian minerals to evaluate the mineral chemical variation in granites to understand the source characteristics and tectonic setting (Elliott 2001; Kumar and Pathak 2010). The composition and texture of amphibole are sensitive to pressure, temperature, and bulk composition and can be used as potential proxies for the qualitative and quantitative estimation of magmatic processes and crystallization parameters (Bachmann and Dungan 2002; Mutch *et al.* 2016). The Al-in amphibole (hornblende) is widely used to estimate the depth of emplacement of calc-alkaline plutons (Hammarstrom and Zen 1986; Ghent *et al.* 1991; Vyhnal *et al.* 1991). The chemical composition of amphibole controls the bulk composition, temperature, pressure, oxygen fugacity, and water content of the source magma (Schmidt 1992; de Oliveira *et al.* 2010; Ridolfi *et al.* 2010). The crystallization stability of amphibole is dependent on the water content of the melt and has been used to estimate the actual H_2O content of parental magma (Naney 1983; Dall'Agnol *et al.* 1999; Parat *et al.* 2008; de Oliveira *et al.* 2010).

Biotite, another hydrous ferromagnesian rock-forming silicate mineral is structurally and chemically highly sensitive and can accommodate most of the major elements (Mg, Fe, Al, K, Si, O, Ti, and F) in the host magma depending upon the prevailing physico-chemical conditions such as pressure, temperature, oxygen fugacity, and composition (Wones and Eugster 1965; Czamanske and Wones 1973; Czamanske *et al.* 1977; Speer 1987). Biotite has the potential crystal structure to reflect the nature and physico-chemical conditions of host felsic magma from which it is formed by accommodating and substituting chemical elements from the felsic magma (Abdel-Rahman 1994; Machev *et al.* 2004; Kumar and Pathak 2010). The annite (Fe^{2+}) and oxynite (Fe^{3+}) components in biotite strongly suggest redox conditions of host felsic magma. Also, they indicate magnetite- and ilmenite-series granites (Ishihara 1977) corresponding to bimodal I- and S-type granites, respectively (Chappell and White 1974). Due to the structural and chemical sensitivity of amphibole and biotite, they can be used as potential proxies to understand the physico-chemical conditions and tectono-magmatic evolution of granitic magma (Wones and Eugster 1965; Ishihara 1977; Abdel-Rahman 1994; Ridolfi *et al.* 2010). The northeastern part of the Eastern Dharwar Craton (EDC) hosts abundant unclassified granitoids of the Neoarchean age. Granites from the Nizamabad region constituting the northeastern part of EDC are relatively less known, mostly limited to field and petrographic observations. This study aims to assess physico-chemical conditions (i.e., temperature, pressure, oxygen fugacity (log-fO_2), H_2O content), magma evolution, and tectonic setting.

2. Geology of the Dharwar Craton and field relationships

The Dharwar Craton (DC) (figure 1a) (Geological Survey of India 1996) is one of the well-studied cratonic blocks of southern India (Chadwick *et al.* 2000; Moyen *et al.* 2003; Jayananda *et al.* 2018).

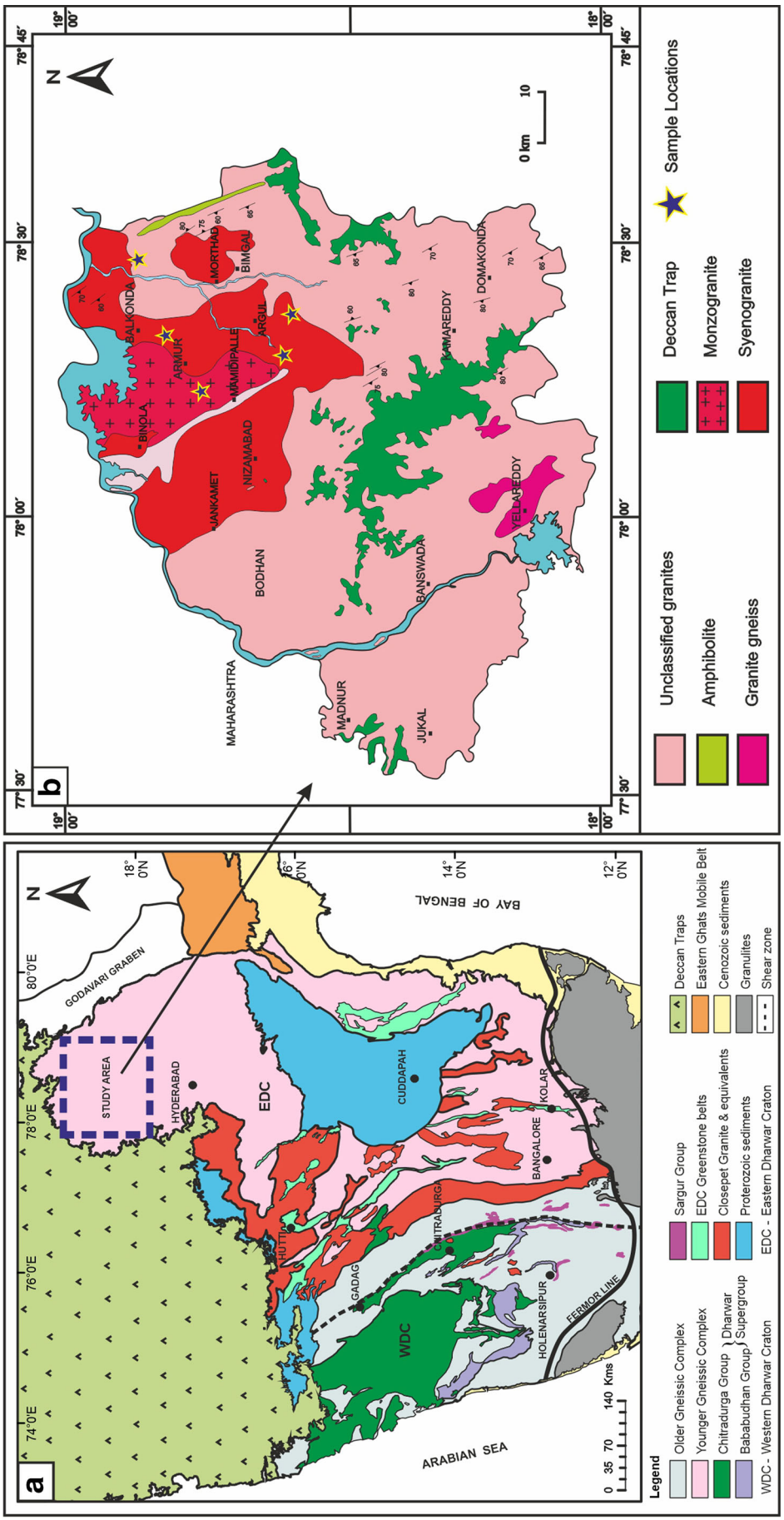

Figure 1. (**a**) Generalized geological map of the Dharwar Craton (after Geological Survey of India 1996) showing two cratonic blocks; older Western Dharwar Craton and younger Eastern Dharwar Craton, the study area Nizamabad is located in the northeastern part of the Eastern Dharwar Craton (marked in the map). (**b**) Generalized geological map of Nizamabad district (after Geological Survey of India 1971) showing the undifferentiated granite gneisses and granitoids of Neoarchean age, along with Cretaceous Deccan lava flows. Sample locations are marked in figure 1(b).

Deccan basalts overlie the northern boundary of the DC, and the southern margin is marked by high-grade Southern Granulite Terrain (SGT). The western and eastern margins are bordered by the Western and Eastern Ghats, respectively. Based on lithological associations, age, and crustal thickness, the DC is divided into two cratonic blocks, namely the Western Dharwar Craton (WDC) and the Eastern Dharwar Craton (EDC) (Swaminath *et al.* 1976; Chardon *et al.* 2008). The steep mylonitic zone along the eastern margin of the Chitradurga Greenstone Belt marks the boundary between the EDC and WDC. Based on the age of basement rocks and grade of metamorphism, and the isotopic data, the EDC is further divided into the central and eastern provinces (Peucat *et al.* 2013).

The Dharwar Craton constitutes Paleo to Neoarchean crustal blocks that record complex and diverse tectonic processes (Jayananda *et al.* 2018). The DC is primarily made up of different types of gneisses, two generations of greenstone successions, and calc-alkaline to potassic granitoid plutons. The WDC comprises tonalite–trondhjemite–granodiorite gneiss that was emplaced episodically between 3.44 and 3.10 Ga and are variably deformed (Jayananda *et al.* 2015; Ranjan *et al.* 2020). The greenstone successions of the DC are divided into the older Sargur Group and the younger Dharwar Supergroup (Ramakrishnan and Vaidyanathan 2008). The Sargur Group greenstones and interlayered TTG gneisses form the basement for the younger Dharwar Supergroup (Jayananda 2013). The older Sargur Group is mostly composed of supracrustals, i.e., Paleo- to Mesoarchean bimodal volcanics interspersed with meta-sedimentary units of quartz–pelite–carbonate-banded iron formation (Peucat *et al.* 1995; Maya *et al.* 2017; Jayananda *et al.* 2018). The younger Dharwar Supergroup comprises Meso to Neoarchean greenstone successions that unconformably overlies the basement gneisses (Chadwick *et al.* 1981; Srinivasan and Ojakangas 1986; Kumar *et al.* 1996; Jayananda *et al.* 2013). The WDC has undergone multiple crustal reworking events at 3.0 and 2.60 Ga, resulting in younger granitic magmatism (Jayananda *et al.* 2006, 2020).

The Eastern Dharwar Craton is dominated by voluminous granitoids and linear greenstone belts of the Neoarchean age (Manikyamba *et al.* 2017; Jayananda *et al.* 2018, 2020; Mohan *et al.* 2020). Compared to the WDC, the greenstone successions of the EDC are volcanic-dominated and reveal a bimodal age distribution at *ca.* 2.75–2.67 Ga and 2.58–2.54 Ga (Manikyamba and Kerrich 2012; Jayananda *et al.* 2013). However, Meso- to Paleoarchean continental crust in the EDC is revealed by the detrital zircon ages (Maibam *et al.* 2011). Similar to other Archean cratons, the EDC evolution and assembly has been a matter of debate, with the main hypothesis supportive of a plume growth model (Jayananda *et al.* 2000). In contrast, the mutually exclusive subduction model (Chadwick *et al.* 2000) is equally popular. Models involving lateral and vertical tectonics are also envisaged (Harish Kumar *et al.* 2003; Jayananda *et al.* 2013). The southern part of the EDC is relatively well-studied. Based on the isotopic and geochemical characteristics of these rocks, a convergent margin setting has been proposed for its evolution (Balakrishnan *et al.* 1999; Mohan *et al.* 2013). The Neoarchean granitoids from the EDC display great compositional diversity and are divided into TTG, sanukitoids, biotite- and two mica granites, and hybrid granites (Mohan *et al.* 2020). The available U–Pb zircon ages indicate a minor 2.67–2.60 Ga episode of TTG magmatism and a major 2.57–2.52 Ga episode of calc-alkaline granitic emplacement (Jayananda *et al.* 2020; Mohan *et al.* 2020). After the stabilization of the DC, the Archean basement was intruded by numerous mafic dyke swarms of Paleoproterozoic to Mesoproterozoic age (Sarma *et al.* 2020; Yadav *et al.* 2020).

The study area in the Nizamabad region forms the northeastern part of the EDC, and granitoids are the most dominant lithology (figure 1b) (Geological Survey of India 1971). Based on the areal extent and megascopic features, these granitoids are classified into five distinct plutons namely, fine to medium-grained monzogranite (Mamidipally pluton), medium- to coarse-grained syenogranite (Jankampet–Binola pluton), medium-grained leucosyenogranite (Morthad pluton), and Argul and Chillergi plutons (Geological Survey of India 1971).

However, based on field observations (colour, grain size and texture), the most common granite variants from the study area are pink to grey coloured medium- to coarse-grained inequigranular granites, with a variable amount of ferromagnesian minerals such as amphibole and biotite (figure 2a and b). The medium- to coarse-grained pink and grey granites host the microgranular enclaves (ME). Coarse-grained K-feldspar porphyritic granite and fine- to medium-grained monzogranites are also observed (figure 2c and d). The MEs are fine-grained and dominant in mafic phases, vary in size between

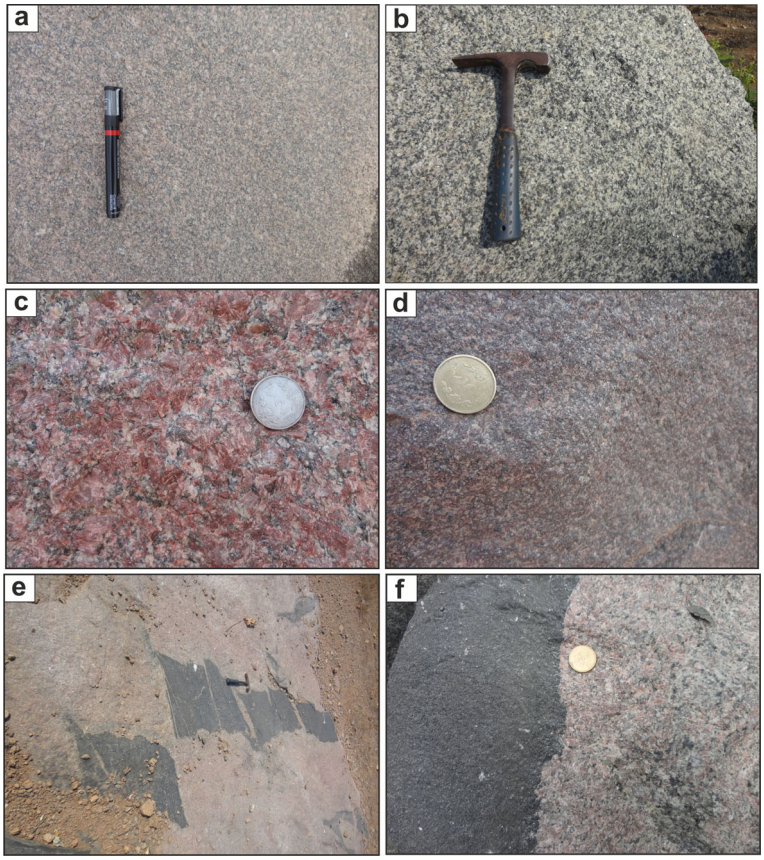

Figure 2. Field photographs of granite variants from the study area. (**a**) Medium to coarse-grained pink granite; (**b**) Medium- to coarse-grained grey granite; (**c**) Coarse-grained K-feldspar porphyritic pink granite; (**d**) Fine-grained pink granite; (**e**) Disintegrated fragments of syn-plutonic mafic dyke intrusions within the host; (**f**) ME displays sharp contact to the host granite.

10 cm and 1 m, and few beyond 10 m (figure 2e and f). These MEs are globular to sub-rounded in shape, and few occur as disintegrated fragments of syn-plutonic mafic dyke intrusions within the host (figure 2e). The coarse-grained K-feldspar porphyritic granite and fine- to medium-grained monzogranites are devoid of MEs and synplutonic mafic dykes. The MEs share sharp boundaries with host granites (pink and grey granites) (figure 2f).

3. Petrography

Based on field observations and detailed petrographic studies, we have divided the studied granitoids into four types, namely, hornblende biotite granites (HBG), biotite granites (BTG), monzogranites (MG), and microgranular enclave (ME).

3.1 *Hornblende biotite granite*

The hornblende biotite granite is essentially composed of quartz, alkali feldspar and plagioclase; the accessory mineral constituents are hornblende, biotite, titanite, epidote, apatite, and opaque minerals (figure 3a). The HBG is texturally inequigranular, and the euhedral alkali feldspars form perthite exsolutions and subhedral plagioclase feldspar exhibits polysynthetic twinning. Hornblende contains inclusions of alkali feldspar, plagioclase, and quartz (figure 3b and c). Apatites are mostly acicular, and few prismatic scraps are also observed. Secondary epidotes are common, whereas primary epidotes are rare and titanites are most commonly associated with mafic minerals like biotite and hornblende, and few allanite crystals are also observed.

3.2 *Biotite granite*

Biotite granites essentially constitute quartz, alkali feldspar, and plagioclase. The accessory phases are biotite, titanite, apatite, zircon, allanite, and opaques (figure 3d). These rocks possess an inequigranular texture with myrmekitic intergrowth and perthite exsolution. Vermicular quartz

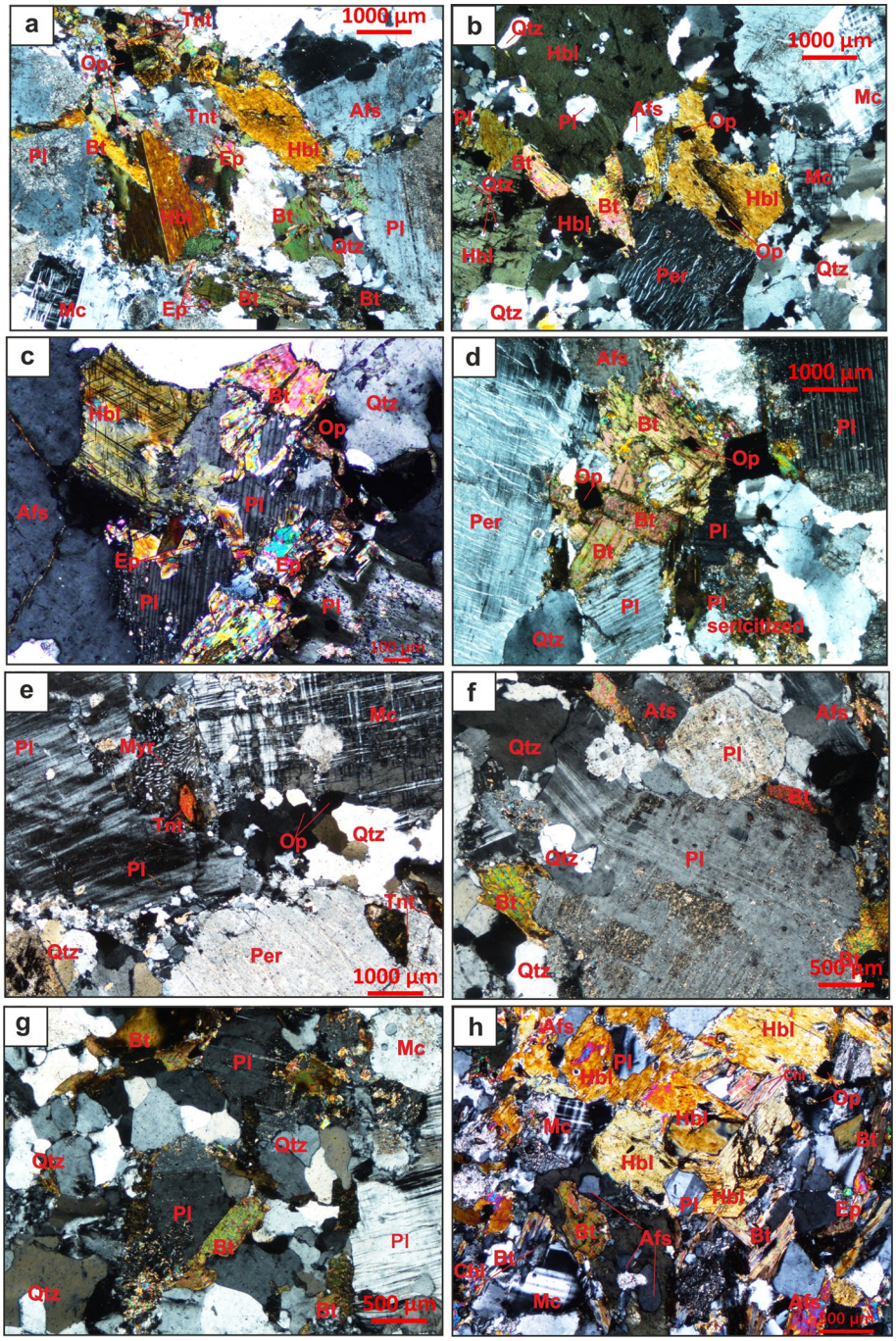

Figure 3. Microphotographs of studied granites depicting the mineral associations and textural features. (**a**) Hornblende biotite granite consists of sericitized plagioclase, alkali feldspar, twinned hornblende, biotite, titanite, epidote, and opaques; (**b**) Hornblende biotite granite shows the perthite exsolution texture, and constitutes of quartz, plagioclase, microcline, hornblende, biotite, opaques. Hornblende contains inclusions of plagioclase, alkali feldspar, and quartz; (**c**) Hornblende biotite granite is composed of quartz, sericitized plagioclase, alkali feldspar, and biotite. Hornblende exhibits conspicuous rhombohedral cleavage; (**d**) Biotite granite shows perthite exsolution texture and essentially constitutes of quartz, alkali feldspar, twinned and sericitized plagioclase, biotite, opaques; (**e**) Biotite granite with myrmekitic texture, microcline display cross-hatched twining, and constitutes of plagioclase, quartz, and titanite; (**f**) Monzogranite comprise plagioclase, quartz, and alkali feldspar with minor biotite; (**g**) The essential minerals in monzogranite are quartz, altered plagioclase, alkali feldspar, and biotite forms the accessory phase; (**h**) ME depicts the clusters of amphiboles and biotites as essential minerals with tabular and prismatic shapes, respectively. Plagioclase, alkali feldspar, quartz, and opaques are accessory phases. Abbreviations. Qtz: quartz, Afs: alkali feldspar, Pl: plagioclase, Mc: Microcline, Hbl: hornblende, Bt: biotite, Per: perthite, Myr: myrmekite, Tnt: Titanite, Ep: epidote, Chl: chlorite, Op: opaque (magnetite).

intergrowth in plagioclase forms myrmekite, and exsolution of albite from microcline results in perthitic exsolution texture (figure 3e). Plagioclase has undergone sericitization and saussuritization, and biotite is altered to chlorite.

3.3 *Monzogranite*

The monzogranite contains quartz, alkali feldspar, and plagioclase as essential minerals, and epidote, apatite, biotite, and titanite are accessory minerals (figure 3f). The monzogranites exhibit inequigranular texture with subhedral plagioclase showing polysynthetic twinning, and the cross-hatched twinning indicates alkali feldspars are microcline. The epidote is found to be confined to altered plagioclases due to saussuritization. Thin biotite prisms occur parallel to the twin lamellae of plagioclase. Biotite, epidote, and opaques form intergranular space between plagioclase grains and alkali-feldspar (figure 3g). The ferromagnesian component of biotite is present as relicts in plagioclase.

3.4 *Microgranular enclave*

The microgranular enclave (MEs) and syn-plutonic mafic dykes are fine-grained with hornblende, biotite, and plagioclase as the major minerals (figure 3h). The accessory phases include alkali feldspar, apatite, epidote, and opaques. The early formed amphiboles occur as clusters within the fine-grained groundmass. The groundmass is composed of biotite, amphibole, plagioclase, and quartz. The amphibole and biotite phenocrysts are subhedral and tabular in shape, whereas they are prismatic and acicular in the groundmass (figure 3h). Plagioclase and microcline display lamellar and cross-hatched twining, respectively. Alteration of plagioclase resulted in the formation of sericite, and chlorite is formed by alteration of biotite. MEs are fine-grained and essentially composed of ferromagnesian minerals (amphibole and biotite) and occur as rounded to sub-rounded. Few occur as syn-plutonic mafic dykes within the host granites. The MEs vary from a few centimeters to >10 m in size and show sharp contact with the host granites. From the contact relationship and relative proportion of mafic minerals, these microgranular enclaves are characterized as mafic microgranular enclaves (MME).

4. Analytical techniques

Fresh representative granitic samples devoid of alteration and weathering rinds were selected for estimating mineral compositions. For the microprobe analysis, thin sections were well polished using diamond paste (Metatech – 1 μm and ¼ μm) and were then carbon coated. The mineral compositions were analyzed using CAMECA SX Five electron microprobe at the Department of Geology, Banaras Hindu University. The analysis was carried out using wavelength dispersive spectrometry with TAP, LiF, LPET, LTAP, and PET crystals. Standards (GeoStd/Di, GeoStd/Prdt, GeoStd/Alm, GeoStd/Ab, GeoStd/Or) are used to calibrate the instrument at a voltage of 15 kV and a current 10 nA with a LaB6 source. SxSAB version 6.1 and SX-Results software were used to carry out routine calibration, acquisition, quantification, and data processing. The precision of the analysis of major element oxides was estimated to be better than 1% from the repeated analysis of standards, and the details are provided elsewhere (Pandey *et al.* 2017).

5. Results

5.1 *Mineral chemistry*

5.1.1 *Plagioclase*

A total of 227 plagioclase compositions were analyzed from representative samples of hornblende biotite granite (HBG), biotite granite (BTG), monzogranite (MG) and microgranular enclave (ME) (Supplementary table S1). The plagioclase composition within the studied granites varies from albite to oligoclase (figure 4). The plagioclase composition in HBG and BTG ranges from (Ab_{98}–Ab_{62} to An_2 –An_{28}) and (Ab_{98}–Ab_{70} to An_5–An_{25}), respectively. Likewise, in MG (Ab_{96}–Ab_{78} to An_2–An_{21}) and ME (Ab_{97}–Ab_{77} to $An_{0.5}$–$An_{5.6}$).

5.1.2 *Alkali feldspar*

A total of 142 alkali feldspar compositions were analyzed, representing HBG, BTG, MG, and ME (Supplementary table S2). The composition of alkali feldspar from studied granites is mostly confined to the field of orthoclase (figure 4). The composition of alkali feldspar in HBG, BTG, MG, and ME ranges from Or_{99} to Or_{95}, Ab_1 to Ab_4, Or_{95}

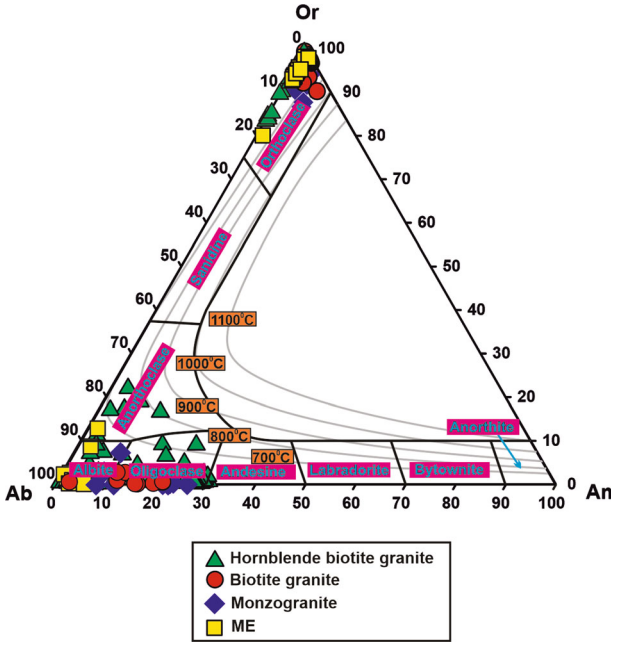

Figure 4. An–Ab–Or ternary feldspar diagram (after Deer *et al.* 1992) depicts crystallization temperature of granitic magma using plagioclase thermometry and compositions of plagioclase, alkali-feldspars from HBG, BTG, ME, and MG.

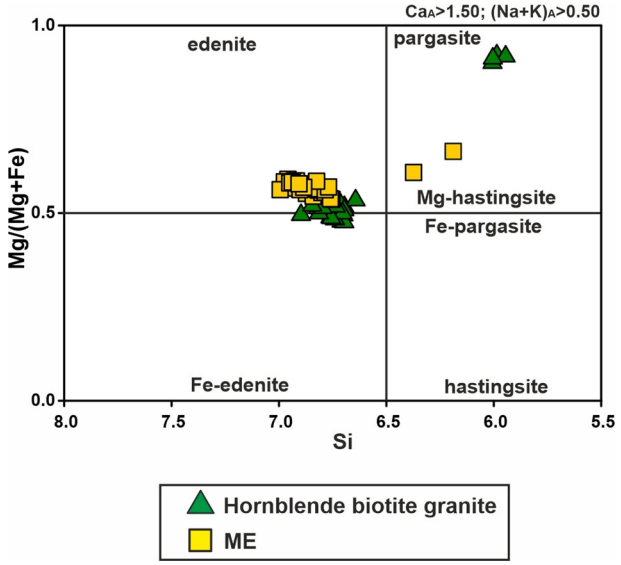

Figure 5. Classification diagram of amphiboles (Leake *et al.* 1997) to exhibit HBG and ME amphibole compositions.

to Or_{99}, $Ab_{0.1}$ to Ab_2, Or_{97} to Or_{95}, Ab_2 to Ab_4, and Or_{95} to Or_{93}, $Ab_{1.2}$ to $Ab_{6.2}$, respectively.

5.1.3 *Amphibole*

A total of 77 amphibole compositions were analyzed from HBG and ME, and only those analyses with totals exceeding 95 wt.% are considered further (Supplementary table S3). The amphibole compositions were calculated based on 23 oxygens, using Geo-fO_2 software (Li *et al.* 2019) and only those analyses where the Ca + Al^{IV} > 2.5 are considered to be primary amphiboles (Giret *et al.* 1980). The total octahedral and tetrahedral cations were adjusted to 13, and then Fe^{3+}/Fe^{2+} ratios were estimated by charge balancing (Leake *et al.* 1997; Ridolfi *et al.* 2010; Li *et al.* 2019). According to the amphibole classification proposed by Leake *et al.* (1997), the amphiboles from HBG and ME are identified as edenite, Fe-edenite, and a few amphiboles from the HBG and ME are falling in the Mg-hastingsite and pargasite fields, respectively (figure 5). The Fe-rich amphiboles represent the rim compositions and iron-enrichment due to alteration along the amphibole rims. The Mg-number (Mg/(Mg + Fe^{+2})) of HGB amphiboles ranges from 0.47 to 0.55 with high Si (5.94–6.89). Amphiboles from the ME exhibit higher Si (6.37–7.72) and Mg-number (53–72) when compared to the HGB amphiboles. The Fe-number (Fe/(Fe + Mg)) of amphiboles within HGB and ME range from 0.27 to 0.44 and 0.44 to 0.52, respectively.

5.1.4 *Biotite*

A total of 90 spots were analyzed from representative HBG, BTG, MG, and ME samples. The structural formula of biotite was calculated based on 22 oxygens, using an excel program designed by Li *et al.* (2020), and is provided in Supplementary table S4. The biotites from HBG, BTG, and MEs are Mg-rich compared to the biotites of MG, which are Fe-rich (figure 6a). On the ternary biotite classification diagram, the Mg-rich biotites are identified as magnesio-biotites, and MG biotites are ferro-biotites (figure 6b). As per Nachit *et al.* (1985) classification, all the studied biotites have re-equilibrated (figure 6c). The negative Al_2O_3–SiO_2 correlations in biotites from HBG, ME, BTG, and MG (figure not shown) infer the accommodation of Al and Si atoms at tetrahedral sites of biotite during magma evolution. This is primarily governed by the change in silica activity (a_{SiO_2}) of parental magma (Abdel-Rahman 1994; Kumar and Pathak 2010). The Fe/(Fe + Mg) ratios increase from ME (0.37–0.40) and HGB (0.37–0.45), towards BTG (0.47–0.52) and MG (0.58–0.66), respectively. The Fe number of hornblende and biotite are similar in the studied HBG and ME. In contrast, a few HBG samples show a higher Fe

number for biotite than those of accompanying amphiboles. The halogen content (Cl and F) in the studied granites reduces from HBG to MG.

5.1.5 *Plagioclase thermometry*

We have used the ternary feldspar isotherm diagram (Deer *et al.* 1992) to estimate the crystallization temperature of granitic magma using plagioclase thermometry (figure 4). The estimated temperatures reveal that the studied granites crystallized over a range of temperature conditions. Feldspars from the HBG are limited to the 600–900°C field, and BTG are confined to 600–800°C. Plagioclases from MG and ME are restricted to 600–700°C (figure 4). Plagioclases from the studied granitoids show more or less similar composition but with contrast in crystallization temperatures.

5.1.6 *Amphibole thermobarometry and hygrometry*

Amphiboles are stable across a wide range of pressure (0.1–25 kbar) and temperature (700–1100°C) conditions; hence, they can be used to effectively estimate the pressure, temperature, water content, and oxygen fugacity of the host magma (Schmidt 1992; Ridolfi *et al.* 2010; Nandedkar *et al.* 2014). We have used the Geo-fO_2 software (Li *et al.* 2019) to estimate the above-mentioned physico-chemical parameters of the studied granites. Based on the amphibole thermometer developed by Ridolfi *et al.* (2010), the

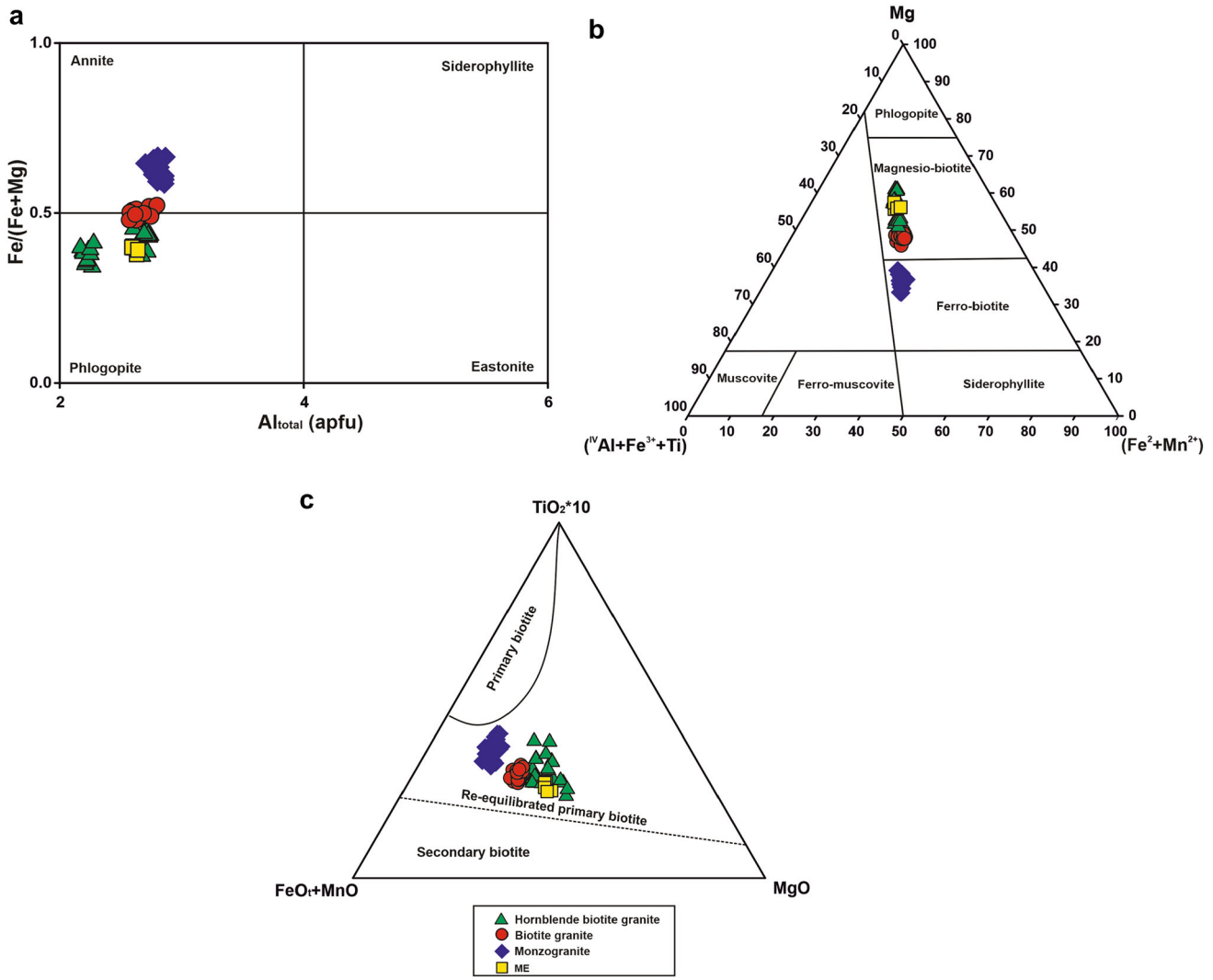

Figure 6. (**a**) Fe/(Fe+Mg) *vs.* $Al_{t(apfu)}$ (Rieder *et al.* 1998) biotite classification diagram; (**b**) (Al^{IV}+Fe^{3+}+Ti)–Mg–(Fe^{2+}+Mn^{2+}) ternary diagram (Foster 1960) showing biotite compositions from HBG, ME, BTG, and MG; and (**c**) 10×(TiO_2)–FeOt + MnO–MgO ternary diagram showing possible origins for biotites from the study area (Nachit *et al.* 1985).

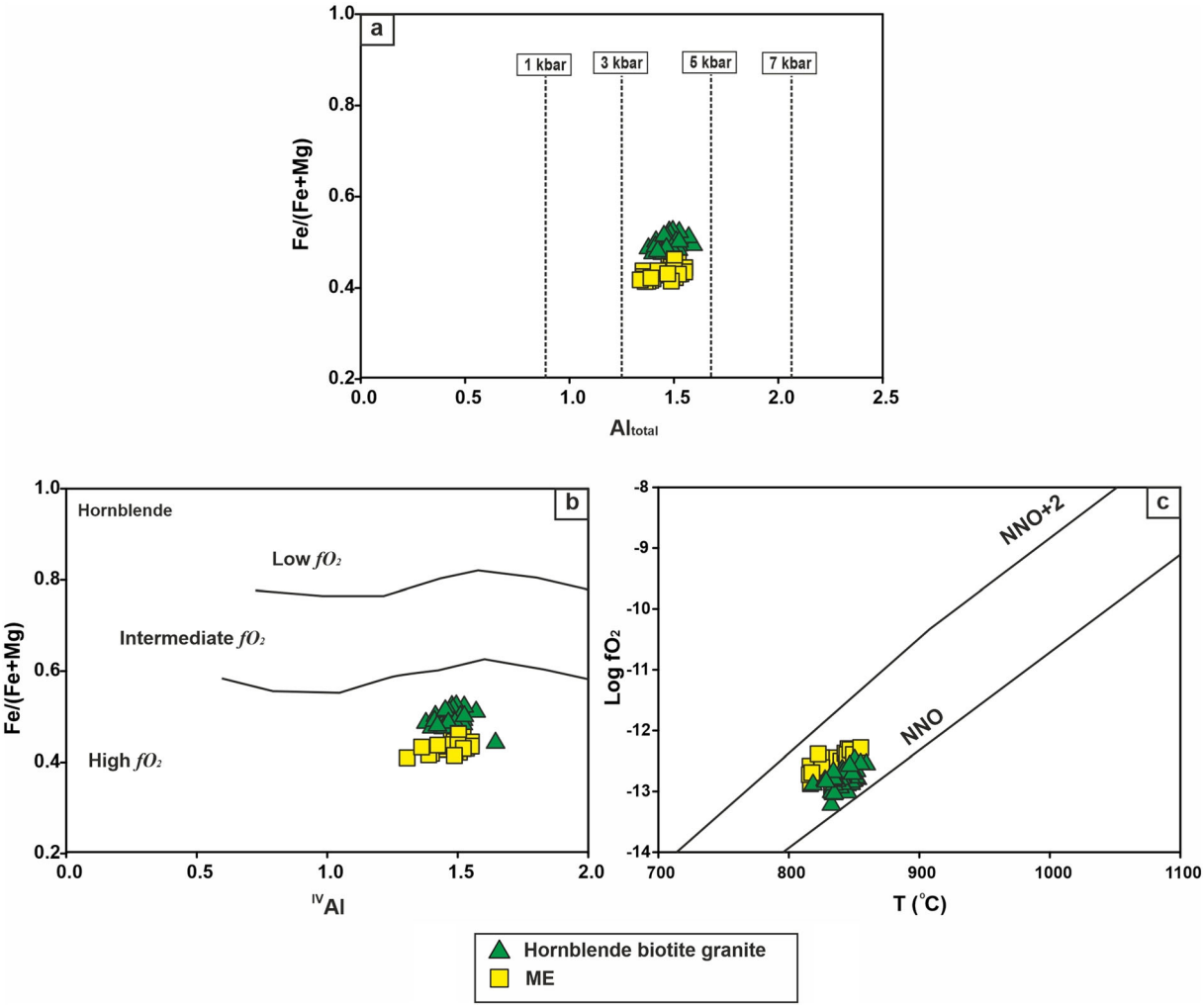

Figure 7. (**a**) Fe/(Fe+Mg) *vs.* Al_{total} diagram (Anderson and Smith 1995) depicts the possible crystallization pressure conditions for amphiboles from HBG and ME; (**b**) Amphibole Fe/(Fe+Mg) *vs.* Al^{IV} diagram (Anderson and Smith 1995) display possible oxygen fugacity (fO_2) conditions for HBG and ME; and (**c**) Log fO_2–T diagram for HBG and ME (Ridolfi *et al.* 2010) infer their amphiboles buffered at NNO (Nickel–Nickel–Oxide).

estimated crystallization temperature for HBG ranges from 818°C to 859 ± 22°C. Whereas those computed for ME mostly range from 800°C to 855 ± 22°C, the average crystallization temperature indicates that both HBG and ME are crystallized under similar conditions (avg. T_{HBG} = 841°C and avg. T_{ME} = 831°C), respectively. Similarly, we used an amphibole geobarometer developed by Schmidt (1992) to estimate the pressure. The results reveal that HBG amphiboles crystallized at pressures between 363 and 448 ± 60 MPa (avg. P_{HBG} = 398 MPa). In contrast, the ME (figure 7a) is crystallized at pressures in the range of 313 to 438 ± 60 MPa (avg. P_{ME} = 386 MPa).

The estimated pressures from amphibole barometry suggest that these granites crystallized at 14–15 km depths, corresponding to upper to mid-continental crust. It has been demonstrated that the amount of Al in the octahedral site of amphibole is sensitive to the water content and can be used to estimate the amount of water in the crystallizing magma (Ridolfi *et al.* 2010). The calculated H_2O content in HBG and ME varies from 4–5 wt.% and 5–6 wt.%, suggesting high water content during the crystallization of these magmas.

5.1.7 *Biotite thermometry*

The Ti contents in biotite are strongly dependent on magma temperature. Using this principle, Henry *et al.* (2005) devised a biotite thermometer to estimate magma temperatures. The application of this thermometer is strictly valid when the X_{Mg} = Mg/(Mg + Fe) = 0.275–1.000, Ti = 0.04–0.60 apfu based on 22 oxygens and the upper limit of

temperature is 800°C. The biotites from HBG (X_{Mg} = 0.65–0.54 and Ti = 0.23–0.06), BTG (X_{Mg} = 0.52–0.47 and Ti = 0.15–0.13), MG (X_{Mg} = 0.41–0.33 and Ti = 0.25–0.17), and ME (X_{Mg} = 0.62–0.59 and Ti = 0.13–0.11) satisfies the above conditions. The estimated temperatures using biotite thermometry shows a higher temperature for HGB and ME (838 to 856 ± 12°C and 844 to 847 ± 12°C) and slightly lower temperature for BTG and MG (829 to 830 ± 12°C and 820 to 829 ± 12°C). The temperature estimates of ME and HBG using amphibole thermometry and biotite thermometry are more or less similar. As stated above, the upper limit for the validity of biotite thermometry is 800°C; these values may not correspond to the actual magma crystallization temperatures.

5.1.8 *Oxygen fugacity (fO_2)*

There are different techniques to estimate the oxygen fugacity of granitic magmas, such as zircon rare earth element systematics (Burnham and Berry 2014), the chemical composition of amphibole and biotite (Wones and Eugster 1965; Anderson and Smith 1995; Ridolfi *et al.* 2010). The oxygen fugacity (fO_2) conditions of amphibole from the HBG and ME are calculated using Geo-fO_2 software, based on the technique developed by Ridolfi *et al.* (2010). The disposition of the HBG and ME amphiboles on the Al^{IV} *vs.* Fe/(Fe + Mg) diagram (Anderson and Smith 1995) indicates that these granites crystallized under high oxygen fugacity (fO_2) conditions (figure 7b) and are confined to the field of NNO buffer (figure 7c). The estimated oxygen fugacity (log fO_2) conditions for HBG and ME are –12.93 to –12.36 bar and –12.89 to –12.11 bar, respectively. The mineral assemblage of the studied granites and ME include amphibole, biotite, K-feldspar, plagioclase, magnetite, and titanite. The ternary Fe^{+2}–Fe^{+3}–Mg diagram is widely used to estimate oxygen fugacity (fO_2) from biotite compositions (Foster 1960). Here, the field of QFM (Quartz–Fayalite–Magnetite), NNO (Nickel–Nickel–Oxide), and HM (Hematite–Magnetite) buffers correspond to an increase in fO_2 from QFM to HM (figure 8a). The biotite compositions from the Nizamabad granites indicate that these magmas are crystallized under NNO buffer. The binary Al^{T} *vs.* Fe/(Fe + Mg) diagram infers that the biotite compositions from the studied granites are corresponded to magnetite-series granites (oxidised) and exhibit decreasing oxidised trends from HBG to MG (figure 8b). Further, we have estimated the oxygen fugacity with biotite stability at isobaric conditions (P = 2070 bar) using the technique of Wones and Eugster (1965). The HBG and ME reveal higher oxygen fugacity (log fO_2) conditions –13.22 to 13.01 bar and –13.12 to 13.09 bar, whereas BTG and MG exhibit slightly lower log fO_2 conditions –13.38 to –13.30 bar and –13.57 to –13.39 bar, and display a reducing trend of oxygen fugacity (log fO_2) from HBG to MG (figure 8c).

6. Discussion

6.1 *Physico-chemical conditions of granitic emplacement*

6.1.1 *Temperature and pressure*

The estimated crystallization temperatures for granitic magma using plagioclase thermometry display a range of crystallization temperatures (figure 4) for the studied granites and MEs. Plagioclase from the HBG shows comparatively higher temperatures, limited to 600–900°C, and BTG are confined to 600–800°C. The plagioclase from MG and ME display slightly lower temperatures and restricted to 600–700°C. The amphibole thermometry of HBG and ME suggest overlapping crystallization temperatures between 818°C and 859 ± 22°C and 800°C to 855 ± 22°C for HBG and ME, respectively (avg. T_{HBG} = 841°C and avg. T_{ME} = 831°C). The calculated temperatures using biotite thermometry show the higher temperature for HGB and ME (838 to 856 ± 12°C and 844 to 847 ± 12°C) and slightly lower temperatures for BTG and MG (829 to 830 ± 12°C and 820 to 829 ± 12°C). The temperature estimates of ME and HBG using amphibole thermometry and biotite thermometry are more or less similar. The observed similarity in temperatures of HBG and ME suggest the cotectic crystallization temperature range of plagioclase and hornblende (Holland and Blundy 1994; Moazzen and Droop 2005).

The obtained amphibole geobarometry reveals that HGB amphiboles are crystallized at pressures between 363 and 448 ± 60 MPa (avg. P_{HBG} = 398 MPa). In contrast, the MEs are crystallized at pressures between 313 and 438 ± 60 MPa (avg. P_{ME} = 386 MPa). The observed lower pressure of ME is possibly due to the undercooling of within-host granite melts

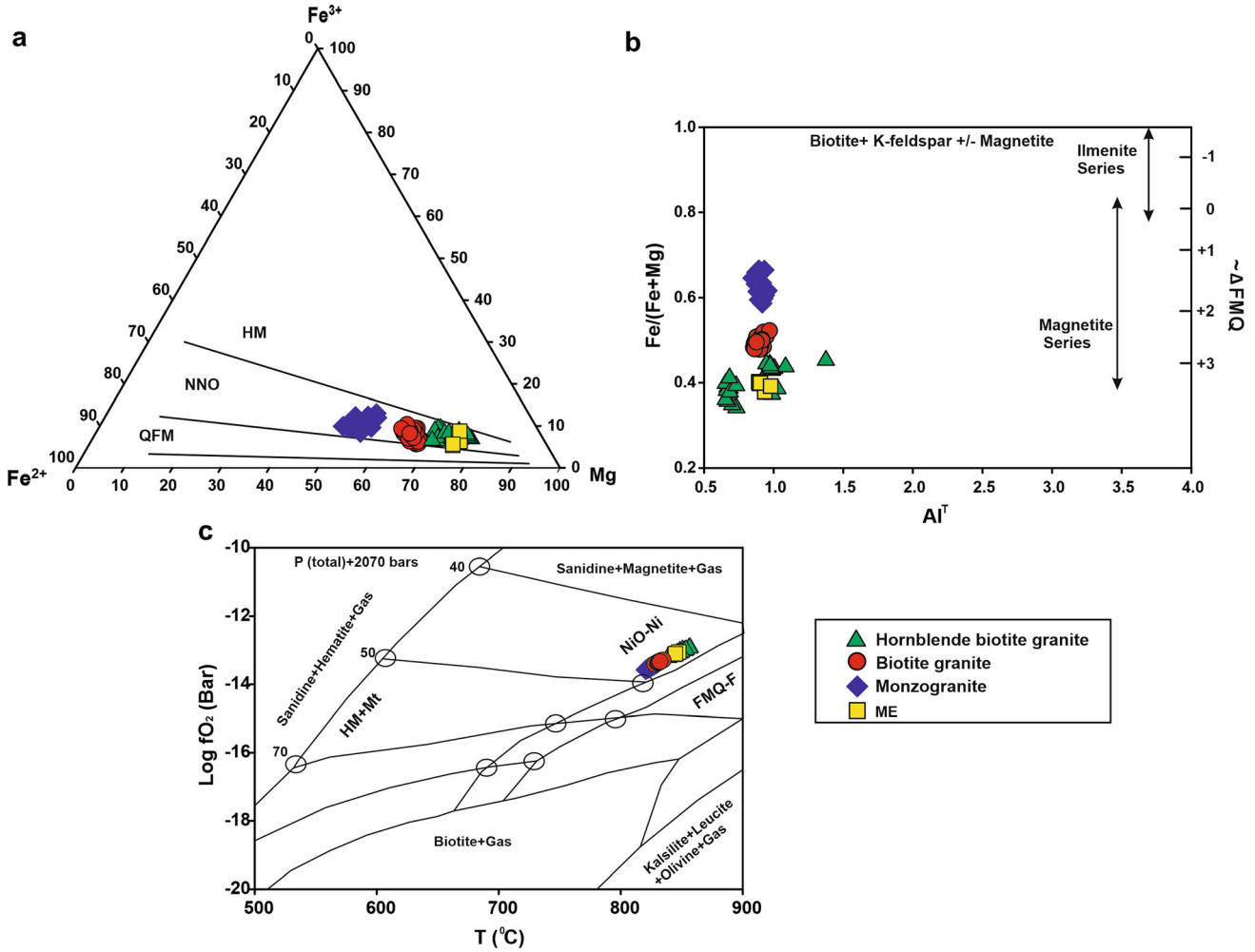

Figure 8. (**a**) Fe^{+2}–Fe^{+3}–Mg ternary diagram (Foster 1960) wherein the biotites indicate NNO buffer field for studied granites (NNO: Nickel–Nickel–Oxide, QFM: Quartz–fayalite–magnetite, HM: Hematite–magnetite); (**b**) The Al_{total} *vs.* Fe/(Fe+Mg) diagram (Foster 1960) displays the oxidized (magnetite series) conditions for HBG, ME, BTG and slightly reduced (low-oxidized) conditions for MG; (**c**) Temperature (°C) *vs.* log fO_2 (bar) diagram, of biotite stability at isobaric condition (P=2070) (Wones and Eugster 1965) showing oxygen fugacity (fO_2) conditions for studied granites (HBG, BTG, and MG) and ME.

(HBG and BTG) at comparatively higher oxidation conditions (Kumar 2010; Bora and Kumar 2015). Alternately, long-term interactions between mafic and felsic end-members and subsequent re-equilibration can also lower the pressure among ME (Kumar and Rino 2006; Kumar 2010; Bora and Kumar 2015). The estimated pressures suggest that these granites have been crystallized at depths of 14–15 km, corresponding to the upper to mid-continental crust.

6.1.2 *Oxygen fugacity and water content*

The estimated oxygen fugacity (log-fO_2) conditions using amphibole compositions for HBG and ME are –12.93 to –12.36 bar and –12.89 to –12.11 bar, respectively. The estimated oxygen fugacity (log-fO_2) conditions from biotite stability at isobaric pressure ($P = 2070$ bar) display higher oxygen fugacity (log fO_2) conditions for HBG (–13.22 to –13.01 bar) and ME (–13.12 to 13.09 bar), whereas BTG and MG exhibit slightly lower log-fO_2 conditions (–13.38 to –13.30 bar) and (–13.57 to –13.39 bar) (figure 8c).

The presence of opaque (Fe–Ti oxides) and ferromagnesian minerals (amphibole and biotite) account for the high fO_2 conditions in granitic rocks (Czamanske and Wones 1973; Czamanske *et al.* 1977, 1981; López-Moro and López-Plaza 2004). The inferred oxidizing conditions based on biotite stability at isobaric pressure ($P = 2070$ bar) from the *T vs.* fO_2 diagram (figure 8c) exhibit high oxidizing conditions for HBG, ME compared to BTG, and are consistent with the modal

abundance of magnetite, titanite, and ferromagnesian minerals. These granites are confined to the field of NNO buffer (high log-fO_2), inferring high oxidizing conditions (figure 8a), and confined to granites of magnetite series (figure 8b). In contrast, the MGs display less log-fO_2 compared to HBG, ME, BTG and have evolved under a slightly reduced (low-oxidized) environment with a minor content of ferromagnesian minerals and Fe–Ti oxides and exhibit decreasing oxidised trend from HBG to MG (figure 8b). The absence of amphibole, negligible amount of biotite, and Fe–Ti oxides in MG depict magma evolution's typical reducing trend (figure 8c).

The calculated H_2O content using Al-content in amphibole for HBG and ME varies between 4–5 and 5–6 wt.%, respectively, suggesting high water content during the crystallization of these magmas. It is well established that the crystallization stability of amphibole is highly dependent on the H_2O content of a melt (Naney 1983; Dall'Agnol *et al.* 1999; Parat *et al.* 2008; de Oliveira *et al.* 2010). The petrographic studies of HBG and ME reveal the early crystallization of amphibole with euhedral nature containing inclusions of quartz, K-feldspar, biotite, and plagioclase and the absence of relict pyroxenes. The abundant modal proportion of amphibole in the HBG and ME suggests high H_2O content during the crystallization of magma. The experimental data infer that 5 wt.% of H_2O content required at 400 MPa and/or H_2O content of 7–9 wt.% needed at 960 MPa, for amphibole to be in liquidus silicate phase and to disappear the pyroxene (Naney 1983; Prouteau and Scaillet 2003; de Oliveira *et al.* 2010). This high H_2O content is further evident by the pervasive sub-solidus alteration that affected the studied rocks and accounted for the intense saussuritization of plagioclase (figure 3a–d) (de Oliveira *et al.* 2010). The water-rich and highly oxidizing conditions for HBG, BTG and ME and slightly reducing conditions for MG infer the upper crustal origin for the Nizamabad granites.

6.2 *Magma evolution and tectonic setting*

Based on the available bulk rock geochemical data, the granitoids of the EDC have been divided into TTG, sanukitoids, biotite- and two mica granite and hybrid granites (Mohan *et al.* 2020). The modal abundance of alkali feldspar in all the granitoid variants is on par or exceeds the plagioclase, confirming these rocks are not TTGs. The mineral assemblage of the HBG, including the close association of MEs and syn-plutonic mafic dykes, hint towards their sanukitoid affinity and possible mantle contribution. The MGs are poor in ferromagnesian mineral phases and show affinity towards the crustal origin. The I-type granites generally contain calcic amphiboles, whereas, in A-type granites, amphiboles would be sodic rich (Stein and Dietl 2001). The higher Fe/Fe + Mg ratios (>0.65) are often associated with anorogenic granites that crystallize under low oxygen fugacity conditions (Anderson and Smith 1995). In the case of HBG and ME, the avg. Fe/Fe + Mg ratios are 0.47 and 0.41, respectively. The magma composition from which amphiboles have crystallized can be depicted by SiO_2 *vs.* TiO_2 plot (Droop 1987). The amphiboles that crystallize from alkaline and ultramafic magmas would be Ti-rich compared to calc-alkaline magmas. The amphiboles from the HBG and ME have been distributed into the field of calc-alkaline magma (figure 9a), supporting the above observations. The SiO_2 *vs.* Na_2O diagram of Coltorti *et al.* (2007) can be used to discriminate amphiboles formed in suprasubduction (S) and intraplate (I) settings. The amphibole from HBG and ME are into the S-amph field, further confirming their calc-alkaline nature (figure 9b), and association of these magmas with subduction zones.

Another important tectono-magmatic discriminator was $Al^{IV} = 1.5$, where $Al^{IV} > 1.5$ value denotes the island arc setting, while $Al^{IV} < 1.5$ denotes an active continental margin (Li *et al.* 2014). The observed Al^{IV} values for studied amphiboles from Nizamabad rocks are <1.5, which further attests to subduction affinity. Al_2O_3 and TiO_2 compositions of amphiboles confirm the crust-mantle mixed source for studied rocks (figure 9c) (Changyi and Sanyuan 1984).

The Al_2O_3, FeO_t and MgO compositions in biotite are used to discriminate between different magma type(s) and corresponding tectonic settings (Abdel-Rahman 1994), and suggests that the studied rocks are evolved from calc-alkaline orogenic magma (figure 10a and b). On the source discrimination diagram for biotites (Zhou 1986), the HBG, ME, and BTG are confined to the field of crust-mantle interaction (figure 10c), while the MG are purely crustal derived. This observation is further corroborated by comparatively lower P–T estimates and lower fO_2 values of MG samples (figure 10c).

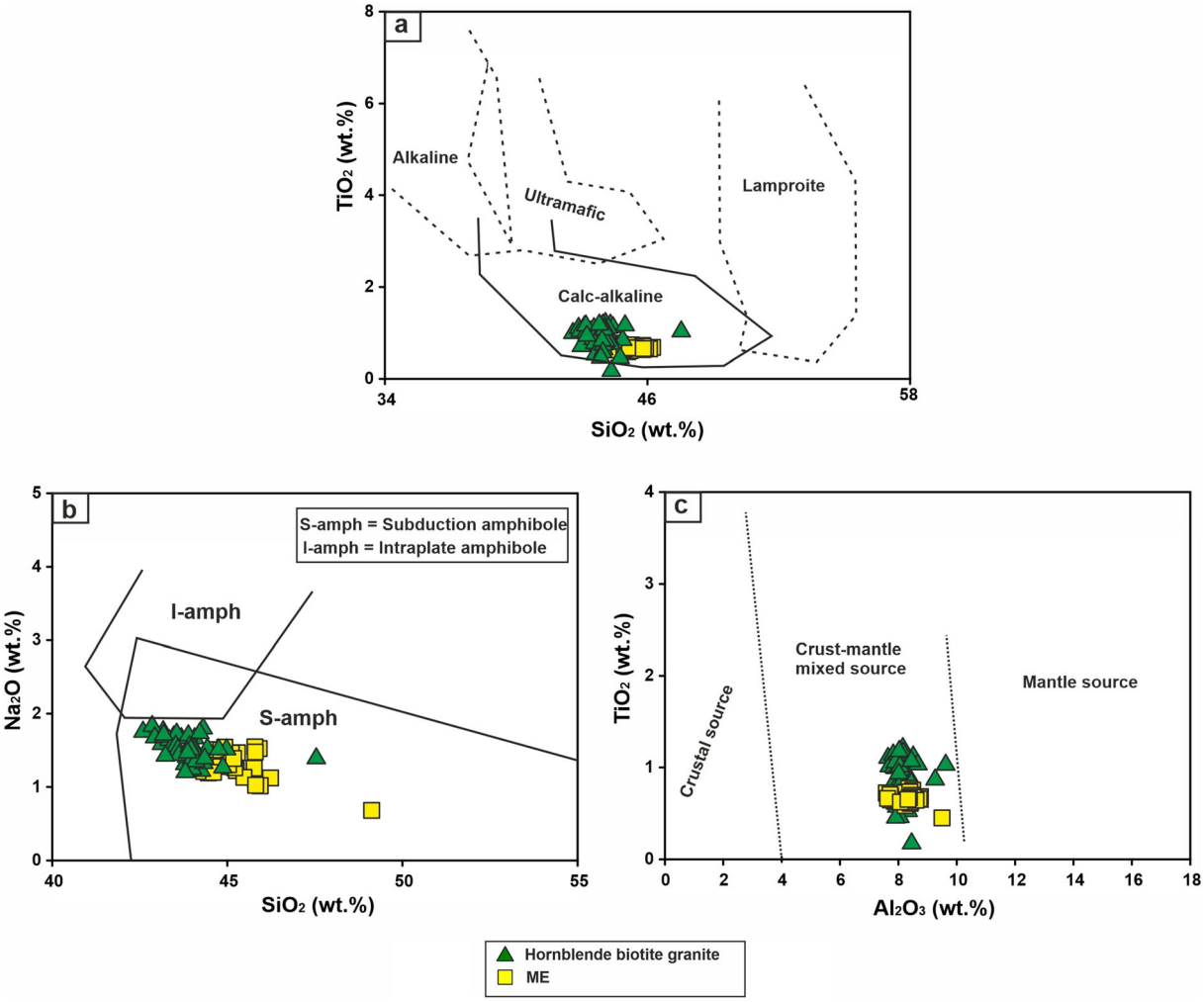

Figure 9. (**a**) SiO_2 *vs.* TiO_2 diagram (Droop 1987) depicts calc-alkaline parental magma for HBG and MEs; (**b**) SiO_2 *vs.* Na_2O diagram of Coltorti *et al.* (2007), show S-amph field for studied granites and ME; (**c**) TiO_2 *vs.* Al_2O_3 (Jiang and An 1984), exhibits crust-mantle mixed source for HBG and ME.

6.3 *Regional implications*

The Dharwar Craton preserved the history of crustal accretion from the Paleoarchean and continued up to Neoarchean (Jayananda *et al.* 2018; Ranjan *et al.* 2020). Along the west to east cross-section, there is a systematic transition from older to younger lithologies and a decline in the involvement of older felsic crust (Mohan *et al.* 2013). The EDC is dominated by voluminous 2.5 Ga potassic calc-alkaline granites and minor 2.6 Ga TTGs, whose evolution is ascribed to a convergent margin tectonic setting (Mohan *et al.* 2013, 2020; Jayananda *et al.* 2018, 2020). The older 2.6 Ga transitional TTGs or hybrid granites were sourced from lower crustal mafic rocks (Dey *et al.* 2017) or from a heterogenous source, involving arc crust and subduction modified mantle (Jayananda *et al.* 2018, 2020), or with the involvement of basaltic source, subduction modified mantle and older felsic crust (Mohan *et al.* 2020). The sanukitoids are syn- to post-collisional and derived from a depleted mantle reservoir enriched in incompatible elements (Heilimo *et al.* 2010; Laurent *et al.* 2014; Jayananda *et al.* 2018, 2020). The biotite and two-mica granites of the EDC were formed at the last stage by reworking of Neoarchean to Paleoarchean felsic crust (Mohan *et al.* 2020).

The mineralogy of different granitic variants at Nizamabad suggests these are akin to potassic granites such as sanukitoids, biotite and two-mica granites, and hybrid granites. The amphibole composition indicates that the HBG and ME are crystallized from water-rich magma. The presence of MEs and synplutonic mafic dykes closely associated with the HBG in the study area indicate the role of mantle-derived magmas. The amphibole composition indicates crust-mantle

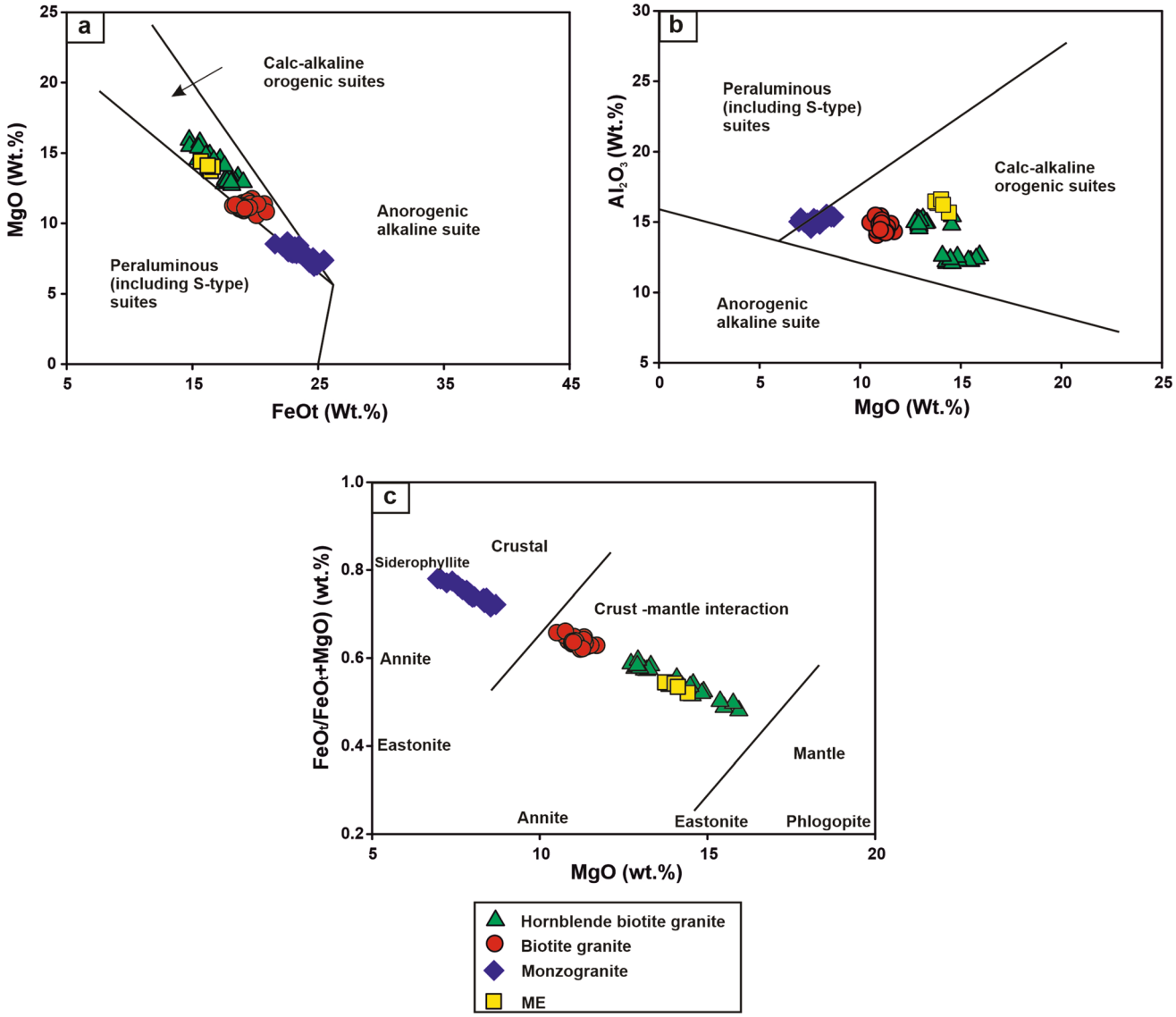

Figure 10. (**a**) FeO^t *vs.* MgO and (**b**) MgO *vs.* Al_2O_3 diagrams (Abdel-Rahman 1994) to discriminate the parental magmatic source for studied granitoids and ME (calc-alkaline, peraluminous, and anorogenic). The biotite compositions indicate the calc-alkaline parental source for studied granitoids. (**c**) MgO *vs.* $FeO_t/(FeO_t+MgO)$ source diagram, conforming the crust-mantle mixed source for HBG, ME, and BTG and crustal source for MG (Zhou 1986).

interactions (figure 10c). The biotite compositions from the different granites indicate significant variation in their magma sources. In the case of MG, their Fe/Fe + Mg ratios are higher than the rest of the granites, indicating reducing conditions. Also, the ferromagnesian minerals such as biotite, hornblende, titanite, ilmenite, and magnetite are the least abundant in MG, indicating their crustal origin. Studies have demonstrated that mineral compositions of pre- to post-collisional granitoids do not exhibit significant variation in their chemistry (Zarasvandi *et al.* 2019). Hence, it may be concluded that the granites of the Nizamabad are emplaced in a convergent margin setting. Compositional variability among these granites is ascribed to the differentiation of mantle-derived magma and the reworking of pre-existing felsic crust. However, this issue can be conclusively resolved with bulk rock geochemistry and radiogenic isotopic data.

7. Conclusions

Following are the main conclusions of this study:

(i) Based on mineralogical associations, studied granites are characterized as hornblende biotite granites (HBG), biotite granites (BTG), monzogranites (MG) and microgranular enclaves (ME).

(ii) The estimated thermobarometric conditions of HBG and ME are 818 to 859 ± 22°C and 800 to 855 ± 22°C, respectively, with the pressure of 363 to 448 ± 60 MPa (HBG) and 313 to 438 MPa ± 60 (ME).

(iii) The estimated temperatures using biotite thermometry shows the higher temperature for HGB and ME (838 to 856 ± 12°C and 844 to 847 ± 12°C), slightly lower temperature for BTG and MG (829 to 830 ± 12°C and 820 to 829 ± 12°C).

(iv) The composition of amphibole and biotite suggest their crystallization from calc-alkaline parental magma in subduction setting at high oxygen fugacity (fO_2) conditions.

(v) The water-rich (>5 wt.% H_2O content) and high oxidizing conditions (NNO + 2) of HBG, BTG and ME correspond to magnetite (oxidized) series granites.

(vi) The amphibole and biotite compositions from the Nizamabad granites suggest the crust-mantle mixed source for HBG, ME and BTG, while the MG are purely crustal derived.

(vii) The estimated pressures suggest that these granites crystallized at depths of 14 to 15 km, corresponding to the upper to mid-continental crust.

(viii) The study infers the role of convergent margin tectonics in the emplacement of compositionally variable granites in the NE part of Eastern Dharwar Craton.

Acknowledgements

The authors thank the Director, CSIR-NGRI, for the permission to publish this work (NGRI/Lib/Pub-36). This study forms part of the PhD work of the first author, supported by MLP-6406-28 (DSS) funds. RP acknowledges EPMA facility at Banaras Hindu University, established with a SERB research grant (IR/S4/ESF-18/2011 dated 12.11.2013). Critical comments from an anonymous reviewer helped improve the earlier version of the manuscript.

Author statement

B Vikram Raju: Fieldwork, data interpretation and writing original draft; Ajay Dev Asokan: Fieldwork, data interpretation, writing – review and editing original draft; Rohit Pandey: Methodology, data generation, writing – review and editing; Arathi G Panicker: Fieldwork, data interpretation, writing – review and editing; M Ram Mohan: Conceptualization, supervision, funding acquisition, validation of results, writing –review and editing. All authors have equally contributed to writing this manuscript.

References

Abdel-Rahman A F M 1994 Nature of biotites from alkaline, calc-alkaline, and peraluminous magmas; *J. Petrol.* **35** 525–541.

Altherr R, Holl A, Hegner E, Langer C and Kreuzer H 2000 High-potassium, calc-alkaline I-type plutonism in the European Variscides: Northern Vosges (France) and northern Schwarzwald (Germany); *Lithos* **50** 51–73.

Anderson J L and Smith D R 1995 The effects of temperature and fO_2 on the Al-in-hornblende barometer; *Am. Mineral.* **80** 549–559.

Armstrong R L 1981 Radiogenic isotopes: The case for crustal recycling on a near-steady-state no-continental-growth Earth; *Phil. Trans. Roy. Soc. A* **301** 443–472.

Bachmann O and Dungan M A 2002 Temperature-induced Al-zoning in hornblendes of the Fish Canyon magma, Colorado; *Am. Mineral.* **87(8–9)** 1062–1076.

Balakrishnan S V, Rajamani and G N Hanson 1999 U–Pb ages for zircon and titanite from the Ramagiri area, southern India: evidence for accretionary origin of the eastern Dharwar craton during the late Archean; *J. Geol.* **107** 69–86.

Barbarin B and Didier J 1992 Genesis and evolution of mafic microgranular enclaves through various types of interaction between coexisting felsic and mafic magmas; *Earth Environ. Sci. Trans. Roy. Soc. Edinb.* **83** 145–153.

Belousova E A, Kostitsyn Y A, Griffin W L, Begg G C, O'Reilly S Y and Pearson N J 2010 The growth of the continental crust: Constraints from zircon Hf-isotope data; *Lithos* **119** 457–466.

Bora S and Kumar S 2015 Geochemistry of biotites and host granitoid plutons from the Proterozoic Mahakoshal Belt, central India tectonic zone: Implication for nature and tectonic setting of magmatism; *Int. Geol. Rev.* **57** 1686–1706.

Bowring S A and Williams I S 1999 Priscoan (4.00–4.03 Ga) orthogneisses from northwestern Canada; *Contrib. Mineral. Petrol.* **134** 3–16.

Burnham A D and Berry A J 2014 The effect of oxygen fugacity, melt composition, temperature and pressure on the oxidation state of cerium in silicate melts; *Chem. Geol.* **366** 52–60.

Chadwick B, Ramakrishnan M and Viswanath M N 1981 The stratigraphy and structure of the Chitradurga region: An illustration of cover-basement interaction in the late Archaean evolution of the Karnataka craton, southern India; *Precamb. Res.* **16** 31–54.

Chadwick B, Vasudev V N and Hegde G V 2000 The Dharwar craton, southern India, interpreted as the result of Late Archaean oblique convergence; *Precamb. Res.* **99** 91–111.

Changyi J and Sanyuan A 1984 On chemical characteristics of cal-cic amphiboles from igneous rocks and their petrogenesis significance; *Mineral. Petrol.* **3** 1–9.

Chappell B W 1999 Aluminium saturation in I- and S-type granites and the characterization of fractionated haplogranites; *Lithos* **46** 535–551.

Chappell B W and White A J R 1974 Two contrasting granite types; *J. Pac. Geol.* **8** 173–174.

Chappell B W and White A J R 1992 I- and S-type granites in the Lachlan Fold Belt; *Earth Environ. Sci. Trans. Roy. Soc. Edinb.* **83** 1–26.

Chardon D, Jayananda M, Chetty T R K and Peucat J 2008 Precambrian continental strain and shear zone patterns: South Indian case; *J. Geophys. Res.* **113**.

Chen B, Jahn B M and Wei C 2002 Petrogenesis of Mesozoic granitoids in the Dabie UHP complex Central China: Trace element and Nd–Sr isotope evidence; *Lithos* **60** 67–88.

Coltorti M, Bonadiman C, Faccini B, Grégoire M, O'Reilly S Y and Powell W 2007 Amphiboles from suprasubduction and intraplate lithospheric mantle; *Lithos* **99** 68–84.

Czamanske G K and Wones D R 1973 Oxidation during magmatic differentiation, Finnmarka complex, Oslo Area, Norway: Part 2, the mafic silicates; *J. Petrol.* **14** 349–380.

Czamanske G K, Wones D R and Eichelberger J 1977 Mineralogy and petrology of the intrusive complex of the Pliny Range, New Hampshire; *Am. J. Sci.* **277** 1073–1123.

Dall'Agnol R, Scaillet B and Pichavant M 1999 An experimental study of a lower Proterozoic A-type granite from the Eastern Amazonian Craton, Brazil; *J. Petrol.* **40** 1673–1698.

de Oliveira M A, Dall'Agnol R and Scaillet B 2010 Petrological constraints on crystallization conditions of Mesoarchean sanukitoid rocks, southeastern Amazonian craton, Brazil; *J. Petrol.* **51** 2121–2148.

Deer W A, Howie R A and Zussman J 1992 An introduction to the rock forming minerals; 2nd edn, *Mineral. Mag.* **56** 617–619.

Dey S, Halla J, Kurhila M, Nandy J, Heilimo E and Pal S 2017 Geochronology of Neoarchaean granitoids of the NW eastern Dharwar craton: Implications for crust formation; *J. Geol. Soc. India Spec. Publ.* **449** 89–121.

Dhuime B, Hawkesworth C J, Cawood P A and Storey C D 2012 A change in the geodynamics of continental growth 3 billion years ago; *Science* **335** 1334–1336.

Droop G T R 1987 A general equation for estimating Fe^{3+} concentrations in ferromagnesian silicates and oxides from microprobe analyses, using stoichiometric criteria; *Mineral. Mag.* **51** 431–435.

Elliott B A 2001 Crystallization conditions of the Wiborg rapakivi batholith, SE Finland: An evaluation of amphibole and biotite mineral chemistry; *Mineral. Petrol.* **72** 305–324.

Foster M D 1960 Interpretation of the composition of trioctahedral micas; *USGS Prof. Paper.* **354** 11–48.

Geological Survey of India 1971 Generalised geological map of the Nizamabad district, modified after Geological Survey of India and Indian Space Research Organisation, Bangalore, India.

Geological Survey of India 1996 Generalised Geological Map of India, Project Vasundhara. Geological Survey of India and Indian Space Research Organisation, Bangalore, India.

Ghent E D, Nicholls J, Simony P S, Sevigny J H and Stout M Z 1991 Hornblende geobarometry of the Nelson Batholith, southeastern British Columbia: Tectonic implications; *Canadian J. Asian Earth. Sci.* **28** 1982–1991.

Giret A, Bonin B and Leger J M 1980 Amphibole compositional trends in oversaturated and undersaturated alkaline plutonic ring-composition; *Canad. Mineral.* **18** 481–495.

Hammarstrom J M and Zen E 1986 Aluminum in hornblende: An empirical igneous geobarometer; *Am. Mineral.* **71** 1297–1313.

Harish Kumar S B, Jayananda M, Kano T, Shadakshara Swamy, N and Mahabaleswar B 2003 Late archean juvenile magmatism accretion process in the Eastern Dharwar craton: Kuppam–karimangalam area; *J. Geol. Soc. India Memoir* **50** 375–408.

Henry D J, Guidotti C V and Thomson J A 2005 The Ti-saturation surface for low-to-medium pressure metapelitic biotites: Implications for geothermometry and Ti-substitution mechanisms; *Am. Mineral.* **90** 316–328.

Heilimo E, Halla J and Hölttä P 2010 Discrimination and origin of the sanukitoid series: Geochemical constraints from the Neoarchean western Karelian Province (Finland); *Lithos* **115** 27–39.

Holland T and Blundy J 1994 Non-ideal interactions in calcic amphiboles and their bearing on amphibole–plagioclase thermometry; *Contrib. Mineral. Petrol.* **116** 433–447.

Ishihara S 1977 The magnetite-series and ilmenite-series granitic rocks; *Min. Geol.* **27** 293–305.

Jayananda M 2013 Geochemical constraints on komatiite volcanism from Sargur Group Nagamangala greenstone belt, western Dharwar craton, southern India: Implications for Mesoarchean mantle evolution and continental growth; *Geosci. Front.* **4** 321–340.

Jayananda M, Moyen J F, Martin H, Peucat J J, Auvray B and Mahabaleswar B 2000 Late Archaean 2550–2520 Ma juvenile magmatism in the Eastern Dharwar Craton, southern India: Constraints from geochronology, Nd–Sr isotopes and whole rock geochemistry; *Precamb. Res.* **99** 225–254.

Jayananda M, Chardon D, Peucat J J and Capdevila R 2006 2.61 Ga potassic granites and crustal reworking in the western Dharwar craton, southern India: Tectonic, geochronologic and geochemical constraints; *Precamb. Res.* **150** 1–26.

Jayananda M, Peucat J J, Chardon D, Rao B K, Fanning C M and Corfu F 2013 Neoarchean greenstone volcanism and continental growth, Dharwar craton, southern India: Constraints from SIMS U–Pb zircon geochronology and Nd isotopes; *Precamb. Res.* **227** 55–76.

Jayananda M, Chardon D, Peucat J J and Fanning C M 2015 Paleo- to Mesoarchean TTG accretion and continental growth in the western Dharwar craton, Southern India: constraints from SHRIMP U–Pb zircon geochronology, whole-rock geochemistry and Nd–Sr isotopes; *Precamb. Res.* **268** 295–322.

Jayananda M, Santosh M and Aadhiseshan K R 2018 Formation of Archean (3600–2500 Ma) continental crust in the Dharwar Craton, southern India; *Earth Sci. Rev.* **181** 12–42.

Jayananda M and Aadhiseshan K R *et al.* 2020 Multi-stage crustal growth and Neoarchean geodynamics in the Eastern Dharwar Craton, southern India; *Gondwana Res.* **78** 228–260.

Jiang C Y and An S Y 1984 On chemical characteristics of calcic amphiboles from igneous rocks and their petrogenetic significance; *J. Miner. Petrol.* **03** 19 (in Chinese with English abstract).

Kumar S 2010 Mafic to hybrid microgranular enclaves in the Ladakh batholith, northwest Himalaya: Implications on calc-alkaline magma chamber processes; *J. Geol. Soc. India* **76** 5–25.

Kumar S and Pathak M 2010 Mineralogy and geochemistry of biotites from Proterozoic granitoids of western Arunachal Himalaya: Evidence of bimodal granitogeny and tectonic affinity; *J. Geol. Soc. India* **75** 715–730.

Kumar S and Rino V 2006 Mineralogy and geochemistry of microgranular enclaves in Palaeoproterozoic Malanjkhand granitoids, central India: Evidence of magma mixing, mingling, and chemical equilibration; *Contrib. Mineral. Petrol.* **152** 591–609.

Kumar A, Rao Y J B, Sivaraman T V and Gopalan K 1996 Sm–Nd ages of Archaean metavolcanics of the Dharwar craton, south India; *Precamb. Res.* **80** 205–216.

Laurent O, Martin H, Moyen J F and Doucelance R 2014 The diversity and evolution oflate-Archean granitoids: Evidence for the onset of 'modern-style' plate tectonics between 3.0 and 2.5 Ga; *Lithos* **205** 208–235.

Leake B E and Woolley A R *et al.* 1997 Nomenclature of amphiboles; Report of the subcommittee on amphiboles of the International Mineralogical Association, Commission on New Minerals and Mineral Names; *Canadian Mineral.* **35** 219–246.

Li S R and Santosh M *et al.* 2014 Metallogeny in response to lithospheric thinning and craton destruction: Geochemistry and U–Pb zircon chronology of the Yixingzhai gold deposit, central North China Craton; *Ore Geol. Rev.* **56** 457–471.

Li W, Cheng Y and Yang Z 2019 Geo-fO_2: Integrated software for analysis of magmatic oxygen fugacity; *Geochem. Geophys.* **20** 2542–2555.

Li X, Zhang C, Behrens H and Holtz F 2020 Calculating biotite formula from electron microprobe analysis data using a machine learning method based on principal components regression; *Lithos* **356** 105371.

López-Moro F J and López-Plaza M 2004 Monzonitic series from the Variscan Tormes Dome (Central Iberian Zone): Petrogenetic evolution from monzogabbro to granite magmas; *Lithos* **72** 19–44.

Machev P, Klain L and Hecht L 2004 Mineralogy and chemistry of biotites from the belogradchik pluton-some petrological implications for granitoid magmatism in northwest Bulgaria; *Ann. Sci. Con. Geol.*, pp. 16–17.

Maibam B, Goswami J N and Srinivasan R 2011 Pb–Pb zircon ages of Archaean metasediments and gneisses from the Dharwar craton, southern India: Implications for the antiquity of the eastern Dharwar craton; *J. Earth Syst. Sci.* **120** 643–661.

Manikyamba C and Kerrich R 2012 Eastern Dharwar Craton India: Continental lithosphere growth by accretion of diverse plume and arc terranes; *Geosci. Front.* **3** 225–240.

Manikyamba C, Ganguly S, Santosh M and Subramanyam K S V 2017 Volcano-sedimentary and metallogenic records of the Dharwar greenstone terranes India: Window to Archean plate tectonics, continent growth, and mineral endowment; *Gondwana Res.* **50** 38–66.

Maya J M, Bhutani R, Balakrishnan S and Sandhya S R 2017 Petrogenesis of 3.15 Ga old Banasandra komatiites from the Dharwar Craton, India: Implications for early mantle heterogeneity; *Geosci. Front.* **8** 467–481.

Moazzen M and Droop G T R 2005 Application of mineral thermometers and barometers to granitoid igneous rocks: the Etive Complex, W Scotland; *Mineral. Petrol.* **83** 27–53.

Mohan M R, Piercey S J, Kamber B S and Sarma D S 2013 Subduction related tectonic evolution of the Neoarchean eastern Dharwar Craton, southern India: New geochemical and isotopic constraints; *Precamb. Res.* **227** 204–226.

Mohan M R, Asokan A D and Wilde S A 2020 Crustal growth of the eastern Dharwar craton: A Neoarchean collisional orogeny?; *Geol. Soc. Spec. Publ.* **489** 51–77.

Moyen J F, Martin H, Jayananda M and Auvray B 2003 Late Archaean granites: A typology based on the Dharwar Craton (India); *Precamb. Res.* **127** 103–123.

Mutch E J F, Blundy J D, Tattitch B C, Cooper F J and Brooker R A 2016 An experimental study of amphibole stability in low-pressure granitic magmas and a revised Al-in-hornblende geobarometer; *Contrib. Mineral. Petrol.* **171** 1–27.

Nachit H, Razafimahefa N, Stussi J M and Carron J P 1985 Composition chimique des biotites et typologie magmatique des granitoides; *C.R. Acad. Sci. Sér. 2* **301** 813–818.

Nandedkar R H, Ulmer P and Müntener O 2014 Fractional crystallization of primitive, hydrous arc magmas: An experimental study at 0.7 GPa; *Contrib. Mineral. Petrol.* **167** 1–27.

Naney M T 1983 Phase equilibriua of rock-forming ferromagnesian silicates in granitic systems; *Am. J. Sci.* **283** 993–1033.

Pandey R, Chalapathi Rao N V, Pandit D, Sahoo S and Dhote P 2017 Imprints of modal metasomatism in the post-Deccan subcontinental lithospheric mantle: Petrological evidence from an ultramafic xenolith in an Eocene lamprophyre, NW India; *J. Geol. Soc. London, Spec. Publ.* **463** 117–136, https://doi.org/10.1144/SP463.6.

Parat F, Holtz F and Feig S 2008 Pre-eruptive conditions of the Huerto andesite (Fish canyon system, San Juan volcanic field, Colorado): Influence of volatiles (C–O–H–S) on phase equilibria and mineral composition; *J. Petrol.* **49** 911–935.

Peucat J J, Bouhallier H, Fanning C M and Jayananda M 1995 Age of the Holenarsipur greenstone belt, relationships with the surrounding gneisses (Karnataka, South India); *J. Geol.* **103** 701–710.

Peucat J J, Jayananda M, Chardon D, Capdevila R, Fanning C M and Paquette J L 2013 The lower crust of the Dharwar Craton, Southern India: Patchwork of Archean granulitic domains; *Precamb. Res.* **227** 4–28.

Prouteau G and Scaillet B 2003 Experimental constraints on the origin of the 1991 Pinatubo dacite; *J. Petrol.* **44** 2203–2224.

Ramakrishnan M and Vaidyanathan 2008 Geology of India; Vol. 1, *Geol. Soc. India, Bangalore.*

Ranjan S, Upadhyay D, Abhinay K and Srikantappa C 2020 Paleoarchean and Neoarchean Tonalite–Trondhjemite–Granodiorite (TTG) and granite magmatism in the Western Dharwar Craton, southern India: Implications for Archean continental growth and geodynamics; *Precamb. Res.* **340** 105630.

Ridolfi F, Renzulli A and Puerini M 2010 Stability and chemical equilibrium of amphibole in calc-alkaline magmas: An overview, new thermobarometric formulations and application to subduction-related volcanoes; *Contrib. Mineral. Petrol.* **160** 45–66.

Rieder M, Cavazzini G, D'yakonov Y S, Frank-Kamenetskii V A, Gottardi G, Guggenheim S, Koval P W, Mueller G, Neiva A M, Radoslovich E W and Robert J L 1998 Nomenclature of the micas; *Clay. Miner.* **46** 586–595.

Sarma D S, Parashuramulu V, Santosh M, Nagaraju E and Babu N R 2020 Pb–Pb baddeleyite ages of mafic dyke swarms from the Dharwar Craton: Implications for Paleoproterozoic LIPs and diamond potential of mantle keel; *Geosci. Front.* **11** 2127–2139.

Schmidt M W 1992 Amphibole composition in tonalite as a function of pressure: An experimental calibration of the Al-in-hornblende barometer; *Contrib. Mineral. Petrol.* **110** 304–310.

Speer J A 1987 Evolution of magmatic AFM mineral assemblages in granitoid rocks; the hornblende + melt= biotite reaction in the Liberty Hill Pluton, South Carolina; *Am. Mineral.* **72** 863–878.

Srinivasan R and Ojakangas R W 1986 Sedimentology of quartz-pebble conglomerates and quartzites of the Archean Bababudan Group, Dharwar Craton, South India: evidence for early crustal stability; *J. Geol.* **94** 199–214.

Stein E and Dietl C 2001 Hornblende thermobarometry of granitoids from the Central Odenwald (Germany) and their implications for the geotectonic development of the Odenwald; *Mineral. Petrol.* **72** 185–207.

Swaminath J, Ramakrishnan M and Vishwanathan M N 1976 Dharwar stratigraphic model and Karnataka Craton evolution; *Records Geol. Surv. India* **107** 149175.

Vyhnal C R, McSween H Y and Speer J A 1991 Hornblende chemistry in southern Appalachian granitoids: Implications for aluminum hornblende thermobarometry and magmatic epidote stability; *Am. Mineral.* **76** 176–188.

Wilde S A, Valley J W, Peck W H and Graham C M 2001 Evidence from detrital zircons for the existence of continental crust and oceans on the Earth 4.4 Gyr ago; *Nature* **409** 175–178.

Wones D R and Eugster H P 1965 Stability of biotite: Experiment, theory, and application; *Am. Mineral.* **50** 1228–1272.

Yadav P, Sarma D S and Parashuramulu V 2020 Pb–Pb baddeleyite ages of mafic dykes from the Western Dharwar Craton, Southern India: A window into 2.21–2.18 Ga global mafic magmatism; *J. Asian Earth Sci.* **191** 104–221.

Zarasvandi A, Heidari M, Raith J, Rezaei M and Saki A 2019 Geochemical characteristics of collisional and pre-collisional porphyry copper systems in Kerman Cenozoic Magmatic Arc, Iran: Using plagioclase, biotite and amphibole chemistry; *Lithos* **326** 279–297.

Zhou Z X 1986 The origin of intrusive mass in Fengshandong, Hubei province; *Acta. Petrol. Sini.* **2** 59–70.

Corresponding editor: Rajneesh Bhutani